STABILITY ISSUES OF CONCENTRIC PIPES CONVEYING STEADY AND PULSATILE FLUIDS

Project F004

Report 7

to the

MEMBER COMPANIES OF THE INSTITUTE OF PAPER SCIENCE AND TECHNOLOGY

April 1999

INSTITUTE OF PAPER SCIENCE AND TECHNOLOGY

Atlanta, Georgia

STABILITY ISSUES OF CONCENTRIC PIPES CONVEYING STEADY AND PULSATILE FLUIDS

Project F004

Report 7

A Progress Report

to the

MEMBER COMPANIES OF THE INSTITUTE OF PAPER SCIENCE AND TECHNOLOGY

By

X. Wang and F. Bloom

April 1999

Stability Issues of Concentric Pipes Conveying Steady and Pulsatile Fluids

by

Xiaodong Wang and Frederick Bloom

Executive Summary

This research topic relates directly to the concentric pipe system designs in silo or other mixing units. It has been found that concentric pipe mixers are better than transverse mixers, and are currently used in silo mixing units. We foresee that in the future approach flow system design or modification, concentric pipe mixers will be used even more widely. Because of the fact that concentric pipe mixers have a long suspended inner pipe (often as long as two meters), structure integrity in relation to flow-induced vibration and pipe joint fatigue failure is one of the important design considerations. To properly introduce the subject dealt with in this report, we quickly summarize the research on the vibration of the concentric pipe systems.

The research approaches for this subject are two-fold: firstly, we set out to find the resonance natural frequencies of the suspended pipe coupled with internal and external fluid flows; secondly, we search for potential critical design information when the pipe flows are pulsatile, which is often the case due to pressure pulsations within the pipe flows.

To come up with critical design criteria concerning the dynamical behavior of the tubular beam, we need to vary the pipe lengths, inclination angle, free surface level, flow velocities, and pipe radii. We find that in addition to the introduction of damping effects, the interaction between the inner tubular beam and the internal

and external fluids significantly reduce the natural frequencies. Furthermore, it is found that the longer the outer pipe, the smaller are the natural frequencies of the inner pipe, i.e., the increased confinement of the inner pipe increases its effective (fluid added) mass. We also observe that varying the inner pipe length has a similar, however, much stronger effect on the coupled system frequencies. The physical explanation is that the inner pipe length determines directly the inner pipe structural stiffness and mass (in fact, for a cantilever beam, the natural frequency is inversely proportional to the square of the beam length), and the outer pipe length only contributes to the fluid-structure coupling part. In general, if the structure is more flexible, it is more susceptible to turbulence buffeting as well as to buckling or flutter. We also show that the coupled system frequencies for the given design configuration with different pipe lengths are between the lower and upper bounds calculated for the two cases in which the inner and outer pipes have the same lengths of l and L, respectively. In addition, we find that the lengths of the pipes have a much greater effect on the second coupled system natural frequency than the first one. This result also matches the physical understanding based on the dependence of mode shapes on the pipe length. Interestingly, calculations show that the inclination angle and the depth of the submerged pipe system do not significantly influence the characteristic behavior of the tubular beam. Increasing the inner pipe radius increases the pipe stiffness but also increases the external flow velocity and added mass effects. At some point, the velocity and added mass effects overwhelm the stiffening effect and the inner pipe frequency drops rapidly. In practice we want to avoid the low frequency consistency and pressure variations introduced by the low frequency vibration of the inner pipe, which may not be effectively attenuated. It is also clearly indicated that as the outer pipe diameter increases, for the constant

volume flow rates, the natural frequencies of the inner pipe increase to a plateau. This occurs because reduced confinement lowers the added mass effects on the inner pipe and the external flow velocity decreases until these effects no longer change with increasing outer pipe diameter. To further assist in the design of the pipe system, we also show that the longer the inner pipe, the lower are the natural frequencies of the inner pipe, but the larger are the damping ratios. With the same outer pipe inner diameter, the smaller the inner pipe diameter, the smaller are the natural frequencies of the inner pipe; however, the change of damping ratio is not monotonic and there exists a region around such that the damping ratio is at its lowest level.

In order to obtain the dynamical stability regions, we have to compute the monodromy matrices and their eigenvalues at all parameter spatial grid points within a parameter space subdivided into parameter spatial divisions. Because we do not know *a priori* the structure of the monodromy matrix, and because a poorly constructed monodromy matrix can lead to incorrect conclusions of the dynamical instability, we need to know the critical time step before the numerical integration, and try to avoid the costly trial and error process. With the critical time step problem solved, based on the mathematical model for a submerged concentric pipe system with both unconfined and confined external flows, we have studied both static and dynamic stability issues relating to the pipe system design and obtained some interesting results (elaborated in the coming Report 8 of project F004).

For the steady flow case, we show that the fourth mode is the mode in which, for a sufficiently high value of flow velocity, flutter instability can happen. We note that friction forces have positive effects on avoiding flutter instability, and the longer the outer pipe length, the less likely that flutter will occur. Similarly, friction forces

also have positive effects on delaying the buckling instability. However, the longer the outer pipe length, the more susceptible the inner pipe is to buckling. A more elaborate study on the dependence of the critical buckling velocity on the outer pipe length, friction, and gravitational forces indicates that there exists a transition region. In general, the effects of gravitational forces are not as significant as those of frictional forces.

For the pulsatile flow case, although the numerical Floquet analysis is lengthier than the Bolotin method, it includes both the parametric and combination instabilities. The dynamic instability regions for different cases suggest that gravity and friction effects are not as significant as the outer pipe length with respect to the dynamic stability issues.

We have presented the ranges of both buckling and flutter instability for pipes conveying steady flows for a case study. For the pipes conveying pulsatile fluids, we have also presented two methods to determine the regions of dynamic instability. We find that the outer pipe length is a more important design factor than gravity (relating to inclination angle and submerge depth) and friction. For the inner pipe conveying pulsatile flow, the lowest critical perturbation frequency is nearly twice the second system natural frequency. Although we note that for current pipe system designs with reasonable flow rates, the concentric pipe system is stable, the procedures investigated in this work clearly provide tools in assisting the design or modification of silo piping systems in general.

---

1 Introduction

Fluid conveying pipes are widely used in engineering applications. One of the design challenges is to avoid pipe buckling and flutter under various operation conditions. Initial work on such flow-induced vibration analysis was reported by Ashley and Haviland [2], Benjamin [4] [5], and Paidoussis [10] [13]. A recent survey of this subject is available in Ref. [16].

In the paper industry, one of the key components in approach flow systems is the so-called silo water mixing unit, a cylindrical water storage tank with a constant water level, as depicted in Fig. 1. The inner pipe protruding into the fan pump inlet zone contains a higher consistency fiber stock, and the concentric outer pipe collects the recirculated stock. In addition to the effects on the smooth operation of impellers, the uniformity of stock consistency, and the minimization of pressure variations [22], the turbulent jets coming out of the concentric pipes may introduce severe oscillations in the suspended pipes, which can cause structural damages such as fatigue failure of pipe joints. The flow-induced oscillations associated with the submerged and inclined concentric pipes have been studied in Ref. [21], in which the effects of various design parameters on the natural frequencies and damping ratios are discussed.

In this paper, we consider stability issues relating to such pipe systems. In addition to the divergence (buckling) and oscillatory (flutter) instabilities, we also consider the possible dynamic instability induced by a pulsating flow [8] [15]. Apart from the traditional approach of the Galerkin-Ritz method, with one or two terms for the spatial series expansions, and the Bolotin method [7], we incorporate, in this work, the spatial finite difference approach presented in Ref. [21] along with a direct time integration for the computation of the monodromy matrix. The advantage of

finite difference schemes is to avoid the use of C^1 finite elements or mixed formulations. An elaborate discussion on this subject is available in Refs. [3] and [24]. Based on the eigenvalues of the monodromy matrix, we then deduce the dynamic stability information corresponding to the presence of periodic coefficients. Of course, the physical problem discussed in this paper also possesses some novelties, in particular, discontinuous coefficients introduced by different pipe lengths.

We begin with the mathematical model and its corresponding governing equation in Section 2, and discuss the numerical procedures for the spatial discretization and the construction of the monodromy matrix in Section 3. We present in Section 4 numerical results for a particular pipe system design with both steady and pulsatile flows. As a further check on the numerical results obtained in Section 4, we also offer, in Section 5, an analytical study based on the Bolotin method to compare with the numerical Floquet approach, for a particular pipe system design.

Nomenclature

l	inner pipe length
L	outer pipe length
R_i	inner radius of the tubular beam
R_o	outer radius of the tubular beam
R_e	inner radius of the outer pipe
I	area moment of the tubular beam, $\pi(R_o^4 - R_i^4)/4$
A	cross-sectional area of the tubular beam, $\pi(R_o^2 - R_i^2)$
A_i	inner cross-sectional area of the tubular beam, πR_i^2
A_o	outer cross-sectional area of the tubular beam, πR_o^2
g	gravity
θ	inclination angle
T	axial tension
E	elastic modulus of the pipe
ρ	internal and external fluid densities
U_i	averaged turbulent flow velocity for the internal pipe flow
U_e	averaged turbulent flow velocity for the external pipe flow
ϵ	internal pipe flow velocity perturbation
p_i	internal pipe pressure
p_e	external pipe pressure
D_o	outer diameter of the inner pipe
x_o	entrance distance associated with the turbulent boundary layer

2 The Mathematical Model

Figure 2 shows the mathematical model of the suspended concentric pipe system with the longitudinal direction being that of the x-axis. We assume that the outer pipe is rigid and consider the inner pipe to be a tubular beam. We note that both pipes are submerged in water, and continuous flow between the two concentric cylinders only occurs in the domain $0 \leq x \leq L \leq l$. For the pulsatile inner pipe flow we have $U_i = \bar{U}_i(1 + \epsilon \cos \omega_o t)$, where $\bar{U}_i$, ϵ, and ω_o represent the mean value of the averaged inner pipe flow velocity, the velocity perturbation magnitude, and the perturbation frequency, respectively. According to the discussion in Ref. [15], the inertia term $\rho A_i \dfrac{\partial U_i}{\partial t}$ needs to be added to the axial force equilibrium of the internal flow. By the chain rule, we have for the transverse inertia effects

$$\left(\frac{\partial}{\partial t}+U_i\frac{\partial}{\partial x}\right)^2=\frac{\partial^2}{\partial t^2}+2U_i\frac{\partial^2}{\partial x\partial t}+U_i^2\frac{\partial^2}{\partial x^2}+\frac{\partial U_i}{\partial t}\frac{\partial}{\partial x}. \tag{1}$$

Moreover, we denote the free surface level measured from the origin $(0,0)$ (fixed boundary location for the suspended pipes) as y_o, such that the hydrostatic pressure at the tip of the submerged beam ($x=l$) is given by $\bar{p}=\rho g y_o-\rho g l\sin\theta$; thus we obtain as the expression for the hydrostatic pressure of the external fluid,

$$p_e=(l-x)\rho g\sin\theta-y\rho g\cos\theta+\bar{p}. \tag{2}$$

According to Refs. [11], [14], and [17], we also have the following expression for the hydrodynamic pressure in the concentric flow region,

$$p_o A_o=\frac{1}{2}\rho D_o U_e^2 C_f h(x), \tag{3}$$

where the friction coefficient C_f has, as indicated in Refs. [13], [19], and [20], different values in the confined and unconfined regions, i.e.,

$$C_f=\begin{cases} C_f^1, & 0\le x<L,\\ C_f^2, & L\le x\le l,\end{cases} \tag{4}$$

while

$$h(x)=\begin{cases} \dfrac{R_o}{R_e-R_o}(L-x), & 0\le x<L,\\ 0, & L\le x\le l,\end{cases} \tag{5}$$

and

$$\frac{dh(x)}{dx}=\begin{cases} -\dfrac{R_o}{R_e-R_o}, & 0\le x<L,\\ 0, & L\le x\le l.\end{cases} \tag{6}$$

As discussed in Refs. [11], [13], and [14], the external flow exerts on the tubular beam the following viscous forces per unit length in both the transverse and longitudinal directions,

$$\begin{aligned} f_x^e &= \frac{1}{2}\rho D_o U_e^2 C_f, \\ f_y^e &= -\frac{1}{2}\rho D_o U_e C_f \left(\frac{\partial y}{\partial t} + U_e \frac{\partial y}{\partial x}\right), \end{aligned} \tag{7}$$

where y stands for the transverse displacement of the tubular beam.

Defining the functions $\sigma = 1 + 0.4(x_o/L)C_f^1$ and $\alpha = 0.4C_f^1/\sigma$ for the confined external flow region, we obtain the external fluid inertia forces

$$\begin{aligned} \mathcal{F}_x^e &= 0, \\ \mathcal{F}_y^e &= -\chi\rho A_o \left(\frac{\partial}{\partial t} + \tilde{U}_e \frac{\partial}{\partial x}\right)\left(\frac{\partial}{\partial t} + U_e \frac{\partial}{\partial x}\right) y, \end{aligned} \tag{8}$$

where

$$\chi = \begin{cases} \dfrac{R_e^2 + R_o^2}{R_e^2 - R_o^2}, & 0 \le x < L, \\ 1, & L \le x \le l, \end{cases} \tag{9}$$

and

$$\tilde{U}_e = \begin{cases} U_e(1 - \alpha(x/L)^2)/\sigma, & 0 \le x < L, \\ U_e, & L \le x \le l. \end{cases} \tag{10}$$

Following the derivation in Ref. [21], we obtain the explicit expression for the tension T, based on the assumption that $p_i\,|_{x=l} = \bar{p} - \frac{1}{2}\rho D_o^2 U_e^2 C_b/A$, and the axial force equilibrium at the tip of the tubular beam, i.e., $T\,|_{x=l} = -\bar{p}A + \frac{1}{2}\rho D_o^2 U_e^2 C_b$, where C_b is the coefficient representing the base drag. Abbreviating $-\bar{p}A_o + \frac{1}{2}\rho D_o^2 U_e^2 C_b \frac{A_o}{A}$ as $\mathcal{G}_0$, $(m + \rho A_i)g\sin\theta + \rho A_i \frac{\partial U_i}{\partial t}$ as $\mathcal{G}_1$, and $\frac{1}{2}\rho D_o U_e^2$ as $\mathcal{G}_2$, with m as the mass per-unit length of the inner pipe, we obtain

$$\frac{\partial(T - p_i A_i)}{\partial x} = \mathcal{G}_1 - \mathcal{G}_2 C_f, \tag{11}$$

so that

$$\begin{aligned} T - p_i A_i &= \mathcal{G}_0 + (x-l)\mathcal{G}_1 + \mathcal{G}_2 \int_x^l C_f dx \\ &= \mathcal{G}_0 + (x-l)\mathcal{G}_1 + \mathcal{G}_2 \begin{cases} C_f^1(L-x) + C_f^2(l-L), & 0 \le x < L, \\ C_f^2(l-x), & L \le x \le l. \end{cases} \end{aligned} \tag{12}$$

Thus, in a manner similar to the derivation presented in Ref. [21], we find the following governing equation for $y(x,t)$,

$$c_1 \frac{\partial^4 y}{\partial x^4} + c_2 \frac{\partial^2 y}{\partial x^2} + c_3 \frac{\partial^2 y}{\partial x \partial t} + c_4 \frac{\partial^2 y}{\partial t^2} + c_5 \frac{\partial y}{\partial x} + c_6 \frac{\partial y}{\partial t} = 0, \tag{13}$$

where the coefficients are given by

$$\begin{aligned} c_1 &= EI, \\ c_2 &= \rho A_i U_i^2 - (T - p_i A_i + p_e A_o + \frac{1}{2}\rho D_o U_e^2 C_f h(x)) + \chi \rho A_o \tilde{U}_e U_e, \\ c_3 &= 2\rho A_i U_i + \chi \rho A_o (\tilde{U}_e + U_e), \\ c_4 &= m + \rho A_i + \chi \rho A_o, \\ c_5 &= -(m + \rho A_i - \rho A_o) g \sin\theta + \frac{1}{2}\rho D_o U_e^2 C_f (1 - \frac{dh(x)}{dx}), \\ c_6 &= \frac{1}{2}\rho D_o U_e C_f. \end{aligned} \tag{14}$$

Remark I: For the case of clamped (or built-in) boundary condition at $x = 0$, we have

$$y(0,t) = 0, \qquad \frac{\partial y(0,t)}{\partial x} = 0, \tag{15}$$

while for the free end of the tubular beam at $x = l$, we have

$$\frac{\partial^2 y(l,t)}{\partial x^2} = 0, \qquad EI \frac{\partial^3 y(l,t)}{\partial x^3} + (\bar{p}A - \frac{1}{2}\rho D_o^2 U_e^2 C_b) \frac{\partial y(l,t)}{\partial x} = 0. \tag{16}$$

Remark II: We recognize that the coefficients c_1 to c_6 can be variables depending on the position x. To circumvent the discontinuity at the location $x = L$, where the

confined and unconfined external flow domains are separated, we prescribe a nodal point at that location.

Remark III: For pulsatile flow, only the coefficients c_2 and c_3 are periodic in time with the period $T_o = \frac{\omega_o}{2\pi}$.

Remark IV: Since we focus our attention on the stability issues, we only retain in Eq. (13) the homogeneous part of the governing equation.

3 Stability Analysis

We employ the standard finite difference discretizations to replace the partial differential equation (13) with a set of ordinary differential equations with respect to time. Equivalent difference schemes are also used for the boundary conditions in Eqs. (15) and (16). We define the solution variable $y(x,t)$ at the spatial grid (or nodal) point i as $Y^i(t)$ (depicted in Fig. 3), and its corresponding time derivative as $\dot{Y}^i(t)$. Using an equal spacing h between finite difference stations, and employing the same finite difference approximations as in Ref. [21], we obtain the discretized characteristic equation

node i $(1 \leq i \leq N)$:

$$\begin{aligned} c_4^i \ddot{Y}^i + \frac{c_3^i}{2h}\dot{Y}^{i+1} - \frac{c_3^i}{2h}\dot{Y}^{i-1} + \frac{c_1^i}{h^4}Y^{i+2} + (\frac{c_2^i}{h^2} - \frac{4c_1^i}{h^4} + \frac{c_5^i}{2h})Y^{i+1} + \\ (\frac{6c_1^i}{h^4} - \frac{2c_2^i}{h^2})Y^i + (\frac{c_2^i}{h^2} - \frac{4c_1^i}{h^4} - \frac{c_5^i}{2h})Y^{i-1} + \frac{c_1^i}{h^4}Y^{i-2} + c_6^i\dot{Y}^i = 0. \end{aligned} \tag{17}$$

As the variable coefficients c_1 to c_5 in Eq. (14) could be functions of x they are denoted as c_1^i to c_5^i at the nodal point i. Therefore, Equation (13) becomes

$$\mathbf{M}\ddot{\mathbf{Y}} + \mathbf{C}\dot{\mathbf{Y}} + \mathbf{K}\mathbf{Y} = \mathbf{0}, \tag{18}$$

where $\mathbf{Y}$ is the solution vector, and $\mathbf{M}$, $\mathbf{C}$, and $\mathbf{K}$ stand for the mass, damping (including gyroscopic terms), and stiffness algebraic coefficient matrices, respectively. For the steady flow case, i.e., $\epsilon = 0$, if we assume a characteristic solution $\mathbf{Y} = e^{i\omega t}\widehat{\mathbf{Y}}$, where $\widehat{\mathbf{Y}}$ represents the mode shape with the natural frequency $\omega = 2\pi f$, the stable system corresponds to $Im(\omega) \geq 0$ with $Re(\omega) \neq 0$. We define the buckling instability as $Re(\omega) \longrightarrow 0$ with $Im(\omega) \geq 0$, and the flutter instability as $Im(\omega) < 0$ with $Re(\omega) \neq 0$. Moreover, having the set of second-order ordinary differential equations in Eq. (18), for the case of pulsatile flow, we now introduce a new solution vector $\mathbf{q} = (\mathbf{Y}\ , \dot{\mathbf{Y}})$, and replace Eq. (18) with the following system of $2N$ first-order differential equations with periodic coefficients

$$\dot{\mathbf{q}} = \mathbf{A}(t)\mathbf{q}, \tag{19}$$

where

$$\mathbf{A}(t) = \begin{bmatrix} \mathbf{0} & \mathbf{I} \\ -\mathbf{M}^{-1}\mathbf{K} & -\mathbf{M}^{-1}\mathbf{C} \end{bmatrix}.$$

Of course, the stability analysis of the trivial solution of Eq. (19) also applies to the stability of solutions near the fixed point of the nonlinear dynamical system with the Jacobian matrix $\mathbf{A}(t)$. For this nonautonomous system, the matrix $\mathbf{A}(t)$ has a period T_o. According to the Floquet theory, the fundamental matrix satisfying Eq. (19) can be expressed as the function of a periodic nonsingular matrix $\mathbf{Q}(t)$, with the period T_o, and a constant matrix $\mathbf{D}$,

$$\mathbf{q}(t) = \mathbf{Q}(t)e^{t\mathbf{D}}. \tag{20}$$

Therefore, the eigenvalues of the matrix $\mathbf{D}$, denoted by β, determine the stability of Eq. (19), and we obtain

$$\mathbf{q}(t+T_o) = \mathbf{q}(t)\mathbf{N}, \tag{21}$$

with the monodromy matrix $\mathbf{N} = e^{T_o\mathbf{D}}$.

The eigenvalues of the matrix $\mathbf{N}$, denoted by λ, are related to the eigenvalues β of the matrix $\mathbf{D}$ by

$$\beta = \frac{1}{T_o}(log|\lambda| + iarg\lambda), \quad i = \sqrt{-1}. \tag{22}$$

It is clear that only the real part of β is uniquely defined. If we assign

$$\mathbf{q}(0) = \mathbf{I}, \tag{23}$$

where $\mathbf{I}$ is the identity matrix, we obtain,

$$\mathbf{N} = \mathbf{q}(T_o). \tag{24}$$

In order to derive the monodromy matrix $\mathbf{N}$, we numerically integrate Eq. (19), together with the initial condition (23), using the second-order Runge-Kutta method, i.e.,

$$\mathbf{q}(t+\Delta t) \;=\; \mathbf{q}(t) + \Delta t(\mathbf{k}_1 + \mathbf{k}_2)/2, \tag{25}$$

where

$$\begin{aligned} \mathbf{k}_1 &= \mathbf{A}(t)\mathbf{q}(t), \\ \mathbf{k}_2 &= \mathbf{A}(t+\Delta t)(\mathbf{q}(t) + \Delta t\mathbf{A}(t)\mathbf{q}(t)). \end{aligned}$$

The i^{th} column of the matrix $\mathbf{N}$ corresponds to the numerical solution of Eq. (19) with the i^{th} column of the identity matrix $\mathbf{I}$ as the initial condition. In general, due to the explicit nature of the Runge-Kutta scheme, the construction of the monodromy

matrix can be very expensive. The detailed discussion on the selection of a proper time step is available in Ref. [23].

4 Numerical Results

We study the stability issues for a particular pipe system design with the following physical parameters: $\rho = 1000$ kg/m^3; $m = 2.12$ kg/m^3; $l = 2.392$ m; $L = 1.135$ m; $x_o = 2.4$ m; $y_o = 6.155$ m; $R_i = 0.02$ m; $R_o = 0.025$ m; $R_e = 0.035$ m; $g = 9.8$ m/s^2; $E = 70$ GPa; $C_f^1 = 0.004\pi$; $C_f^2 = 0.5\pi R_i/l$; and $C_b = 0.0125\pi$.

For the steady flow case, Figure 4 shows the loci of the fourth mode in the complex ω plane as a function of the dimensionless velocity $u = \sqrt{\frac{\rho A_i}{EI}} U_i l$, i.e., $U_i = 13.28u$. We find that the fourth mode is the mode in which, for a sufficiently high value of u, flutter instability can happen. We note that friction forces have positive effects on avoiding flutter instability, and the longer the outer pipe length, the less likely that flutter will occur. Similarly, as depicted in Fig. 5, friction forces have positive effects on delaying the buckling instability. However, the longer the outer pipe length, the more susceptible the inner pipe is to buckling. A more elaborate study on the dependence of the critical buckling velocity u_c on the outer pipe length, friction, and gravitational forces indicates, as shown in Fig. 6, that there exists a transition region around $L/l = 0.6$. In general, the effects of gravitational forces are not as significant as those of frictional forces.

For the pulsatile flow case, we denote ω_{oi} as the i^{th} natural frequency of the corresponding steady flow case with both gravity and friction effects. As discussed in Refs. [1], [12], and [18], although the numerical Floquet analysis is lengthier than the Bolotin method, it includes both the parametric ($\omega_o/\omega_{oi} = 2/k, \quad k = 1, 2, 3, ...$) and combination instabilities ($\omega_o/(\omega_{oi} - \omega_{oj}) = 1/k, \quad k = 1, 2, 3, ...$). Figure 7

shows the dynamic instability regions for different cases; as can be seen, gravity and friction effects are not as significant as the outer pipe length l with respect to the dynamic stability issues.

5 Bolotin Method

In this section we consider the case of a pipe system with the same inner and outer pipe length. To simplify the expression for the eigenfunctions satisfying the beam equation and its associated boundary conditions, we ignore frictional forces, the axial load at the tip of the inner tubular beam, and, in general, the gravitational forces. As a consequence of Eq. (12), the forms of $\mathcal{G}_0$ and $\mathcal{G}_1$, and the assumed structure of the pulsatile inner pipe flow, we have

$$T - p_i A_i = (l - x)\rho A_i \bar{U}_i \omega_o \epsilon \sin \omega_o t, \tag{26}$$

while the coefficients c_1 to c_6 in Eq. (14) take on the following form:

$$\begin{aligned} c_1 &= EI, \\ c_2 &= \rho A_i \bar{U}_i^2 (1 + \epsilon \cos \omega_o t)^2 + (x - l)\rho A_i \bar{U}_i \omega_o \epsilon \sin \omega_o t + \chi \rho A_o U_e^2, \\ c_3 &= 2\rho A_i \bar{U}_i (1 + \epsilon \cos \omega_o t) + 2\chi \rho A_o U_e, \\ c_4 &= m + \rho A_i + \chi \rho A_o, \\ c_5 &= 0, \\ c_6 &= 0. \end{aligned} \tag{27}$$

In addition, we may rewrite c_2 and c_3 in the form

$$\begin{aligned} c_2 &= \bar{c}_2 + \tilde{c}_2^1 \epsilon \cos \omega_o t + (x - l)\tilde{c}_2^2 \epsilon \sin \omega_o t + \tilde{c}_2^3 \epsilon^2 \cos 2\omega_o t, \\ c_3 &= \bar{c}_3 + \tilde{c}_3 \epsilon \cos \omega_o t, \end{aligned} \tag{28}$$

with

$$
\begin{aligned}
\bar{c}_2 &= \rho A_i \bar{U}_i^2 (1 + \epsilon^2/2) + \chi \rho A_o U_e^2, \\
\tilde{c}_2^1 &= 2\rho A_i \bar{U}_i^2, \\
\tilde{c}_2^2 &= \rho A_i \bar{U}_i \omega_o, \\
\tilde{c}_2^3 &= \rho A_i \bar{U}_i^2/2, \\
\bar{c}_3 &= 2\rho A_i \bar{U}_i + 2\chi \rho A_o U_e, \\
\tilde{c}_3 &= 2\rho A_i \bar{U}_i,
\end{aligned}
$$

and obtain the following governing partial differential equation:

$$
\begin{aligned}
c_1 \frac{\partial^4 y}{\partial x^4} + (\bar{c}_2 + \tilde{c}_2^1 \epsilon \cos \omega_o t + (x - l)\tilde{c}_2^2 \epsilon \sin \omega_o t + \tilde{c}_2^3 \epsilon^2 \cos 2\omega_o t) \frac{\partial^2 y}{\partial x^2} + \\
(\bar{c}_3 + \tilde{c}_3 \epsilon \cos \omega_o t) \frac{\partial^2 y}{\partial x \partial t} + c_4 \frac{\partial^2 y}{\partial t^2} = 0.
\end{aligned} \tag{29}
$$

We express the solution of Eq. (29) in the form of a series

$$
y(x,t) = \sum_{j=1}^{\infty} a_j(t) \phi_j(x), \tag{30}
$$

where ϕ_j is the j^{th} eigenfunction corresponding to eigenvalue λ_j for the system

$$
\frac{d^4 \phi_j}{dx^4} = \lambda_j^4 \phi_j, \quad 0 < x < l, \tag{31}
$$

with the boundary conditions

$$
\begin{aligned}
\phi_j(0) = \phi_j'(0) = 0, \\
\phi_j''(l) = \phi_j'''(l) = 0.
\end{aligned}
$$

Moreover, the eigenvalue λ_j satisfies the transcendental algebraic equation [6]

$$
1 + \cos \lambda_j l \cos h\lambda_j l = 0, \ j = 1, 2, ... \tag{32}
$$

and the corresponding ϕ_j is given by

$$
\begin{aligned}
\phi_j(x) &= (\cos \lambda_j x - \cos h\lambda_j x) + \sigma_j (\sin \lambda_j x - \sin h\lambda_j x), \\
\sigma_j &= (\sin \lambda_j l - \sin h\lambda_j l)/(\cos \lambda_j l + \cos h\lambda_j l).
\end{aligned} \tag{33}
$$

Of course, we also have the following orthogonal relations

$$\int_0^l \phi_j(x)\phi_k(x)dx = 0, \quad j \neq k, \tag{34}$$

$$\int_0^l \phi_j''(x)\phi_k''(x)dx = 0, \quad j \neq k. \tag{35}$$

Substituting Eq. (30) into Eq. (29), multiplying the resulting equation by $\phi_k(x)$, and integrating from $x = 0$ to $x = l$, we obtain the following equation:

$$c_4\ddot{a}_k + \sum_{j=1}^{\infty}\{(\bar{c}_3 + \tilde{c}_3\epsilon\cos\omega_o t)o_{kj}\dot{a}_j + (\bar{c}_2 + \tilde{c}_2^1\epsilon\cos\omega_o t + \tilde{c}_2^3\epsilon^2\cos 2\omega_o t)p_{kj}a_j + \tilde{c}_2^2\epsilon q_{kj}a_j\sin\omega_o t\} + c_1\lambda_k^4 a_k = 0, \tag{36}$$

where

$$\begin{aligned} \mu_k &= \int_0^l \phi_k^2 dx, \\ o_{kj} &= \int_0^l \phi_k\phi_j' dx/\mu_k, \\ p_{kj} &= \int_0^l \phi_k\phi_j'' dx/\mu_k, \\ q_{kj} &= \int_0^l (x-l)\phi_k\phi_j'' dx/\mu_k. \end{aligned} \tag{37}$$

Notice that some analytical expressions exist for Eq. (37), and in this work, we choose to use numerical integrations. As in Ginsburg [9], we select a two-term series expansion in Eq. (30), i.e., $j = 1, 2$. In this manner, we obtain as the coupled equations for $a_1(t)$ and $a_2(t)$ which result from Eq. (36) the following:

$$c_4\ddot{a}_1 + (\bar{c}_3 + \tilde{c}_3\epsilon\cos\omega_o t)(o_{11}\dot{a}_1 + o_{12}\dot{a}_2) + (\bar{c}_2 + \tilde{c}_2^1\epsilon\cos\omega_o t + \tilde{c}_2^3\epsilon^2\cos 2\omega_o t)(p_{11}a_1 + p_{12}a_2) + \tilde{c}_2^2\epsilon\sin\omega_o t(q_{11}a_1 + q_{12}a_2) + c_1\lambda_1^4 a_1 = 0, \tag{38}$$

$$c_4\ddot{a}_2 + (\bar{c}_3 + \tilde{c}_3\epsilon\cos\omega_o t)(o_{21}\dot{a}_1 + o_{22}\dot{a}_2) + (\bar{c}_2 + \tilde{c}_2^1\epsilon\cos\omega_o t + \tilde{c}_2^3\epsilon^2\cos 2\omega_o t)(p_{21}a_1 + p_{22}a_2) + \tilde{c}_2^2\epsilon\sin\omega_o t(q_{21}a_1 + q_{22}a_2) + c_1\lambda_2^4 a_2 = 0. \tag{39}$$

The coefficients in Eqs. (38) and (39) are periodic with the period T_o and the transition from stability to instability is marked by the existence of a solution with the period T_o or $2T_o$.

The solutions associated with the primary instability at $\omega_o/\omega_{oi} = 2/k, \quad k = 1, 3, 5, ...$ correspond to solutions with the period $2T_o$ and are constructed from the Fourier series:

$$a_i(t) = \sum_{j=1,3,5,...}^{\infty} \left\{ r_{ij} \cos \frac{j}{2}\omega_o t + s_{ij} \sin \frac{j}{2}\omega_o t \right\}, \quad i = 1, 2 \tag{40}$$

while solutions associated with the secondary instability at $\omega_o/\omega_{oi} = 2/k, \quad k = 2, 4, 6, ...$ correspond to solutions with the period T_o and are constructed using the Fourier series:

$$a_i(t) = \frac{1}{2}e_{i0} + \sum_{j=2,4,6,...}^{\infty} \left\{ e_{ij} \cos \frac{j}{2}\omega_o t + f_{ij} \sin \frac{j}{2}\omega_o t \right\}, \quad i = 1, 2 \tag{41}$$

The primary principal instability boundary is generated by solutions of the form (40) with $j = 1$. Thus, truncating the series in Eq. (40), as in Ginsberg [9], we have

$$a_i(t) = r_i \cos \frac{1}{2}\omega_o t + s_i \sin \frac{1}{2}\omega_o t, \quad i = 1, 2 \tag{42}$$

with $r_i \equiv r_{i1}$ and $s_i \equiv s_{i1}$. Substituting Eq. (42) into Eqs. (38) and (39), using various trigonometric relations, and collecting the coefficients of the linearly independent terms $\sin \frac{1}{2}\omega_o t$ and $\cos \frac{1}{2}\omega_o t$, we obtain the system of algebraic equations

$$\begin{bmatrix} M_{11} & M_{12} & M_{13} & M_{14} \\ M_{21} & M_{22} & M_{23} & M_{24} \\ M_{31} & M_{32} & M_{33} & M_{34} \\ M_{41} & M_{42} & M_{43} & M_{44} \end{bmatrix} \begin{bmatrix} r_1 \\ s_1 \\ r_2 \\ s_2 \end{bmatrix} = \begin{bmatrix} 0 \\ 0 \\ 0 \\ 0 \end{bmatrix} \tag{43}$$

where

$$
\begin{aligned}
M_{11} &= -c_4\omega_o^2/4 + \bar{c}_2 p_{11} + \epsilon\tilde{c}_2^1 p_{11}/2 + c_1\lambda_1^4, \\
M_{12} &= \bar{c}_3 o_{11}\omega_o/2 + \epsilon\tilde{c}_3 o_{11}\omega_o/4 + \epsilon\tilde{c}_2^2 q_{11}/2, \\
M_{13} &= \bar{c}_2 p_{12} + \epsilon\tilde{c}_2^1 p_{12}/2, \\
M_{14} &= \bar{c}_3 o_{12}\omega_o/2 + \epsilon\tilde{c}_3 o_{12}\omega_o/4 + \epsilon\tilde{c}_2^2 q_{12}/2; \\
M_{21} &= -\bar{c}_3 o_{11}\omega_o/2 + \epsilon\tilde{c}_3 o_{11}\omega_o/4 + \epsilon\tilde{c}_2^2 q_{11}/2, \\
M_{22} &= -c_4\omega_o^2/4 + \bar{c}_2 p_{11} - \tilde{c}_2^1 p_{11}/2 + c_1\lambda_1^4, \\
M_{23} &= -\bar{c}_3 o_{12}\omega_o/2 + \epsilon\tilde{c}_3 o_{12}\omega_o/4 + \epsilon\tilde{c}_2^2 q_{12}/2, \\
M_{24} &= \bar{c}_2 p_{12} - \tilde{c}_2^1 p_{12}/2; \\
M_{31} &= \bar{c}_2 p_{21} + \epsilon\tilde{c}_2^1 p_{21}, \\
M_{32} &= \bar{c}_3 o_{21}\omega_o/2 + \epsilon\tilde{c}_3 o_{21}\omega_o/4 + \epsilon\tilde{c}_2^2 q_{21}/2, \\
M_{33} &= -c_4\omega_o^2/4 + \bar{c}_2 p_{22} + \epsilon\tilde{c}_2^1 p_{22}/2 + c_1\lambda_2^4, \\
M_{34} &= \bar{c}_3 o_{22}\omega_o/2 + \epsilon\tilde{c}_3 o_{22}\omega_o/4 + \epsilon\tilde{c}_2^2 q_{22}/2; \\
M_{41} &= -\bar{c}_3 o_{21}\omega_o/2 + \epsilon\tilde{c}_3 o_{21}\omega_o/4 + \epsilon\tilde{c}_2^2 q_{21}/2, \\
M_{42} &= \bar{c}_2 p_{21} - \epsilon\tilde{c}_2^1 p_{21}/2, \\
M_{43} &= -\bar{c}_3 o_{22}\omega_o/2 + \epsilon\tilde{c}_3 o_{22}\omega_o/4 + \epsilon\tilde{c}_2^2 q_{22}/2, \\
M_{44} &= -c_4\omega_o^2/4 + \bar{c}_2 p_{22} - \epsilon\tilde{c}_2^1 p_{22}/2 + c_1\lambda_2^4.
\end{aligned}
$$

The existence of the solution of the form (42) corresponds to $detM_{ij} = 0$. Using this criterion, we may obtain the dynamic stability information associated with various design parameters, such as ϵ and ω_o. Figure 8 shows that the results derived from the Bolotin method and the Floquet theory match with each other. The advantage of using the Bolotin method is, of course, its simplicity and efficiency; however, when considering more terms in the series expansions, a derivation based on the Bolotin method can be extensive, and in addition, the Bolotin method is limited to the parametric instability analysis [18].

6 Conclusions

Based on the mathematical model for a submerged concentric pipe system with both unconfined and confined external flows, we have studied both static and dynamic stability issues relating to the pipe system design. We have presented the ranges

of both buckling and flutter instability for pipes conveying steady flows for a case study. For the pipes conveying pulsatile fluids, we have also presented two methods to determine the regions of dynamic instability. We find that the outer pipe length is a more important design factor than gravity (relating to inclination angle and submerge depth) and friction. For the inner pipe conveying pulsatile flow, the lowest critical perturbation frequency is nearly twice the second system natural frequency. However, we note that for current pipe system designs with reasonable flow rates, the concentric pipe system is stable. The procedure implemented in this paper clearly shows much promise in assisting the design for the silo piping system.

7 Acknowledgment

The authors would like to thank the Institute of Paper Science and Technology and its Member Companies for their support.

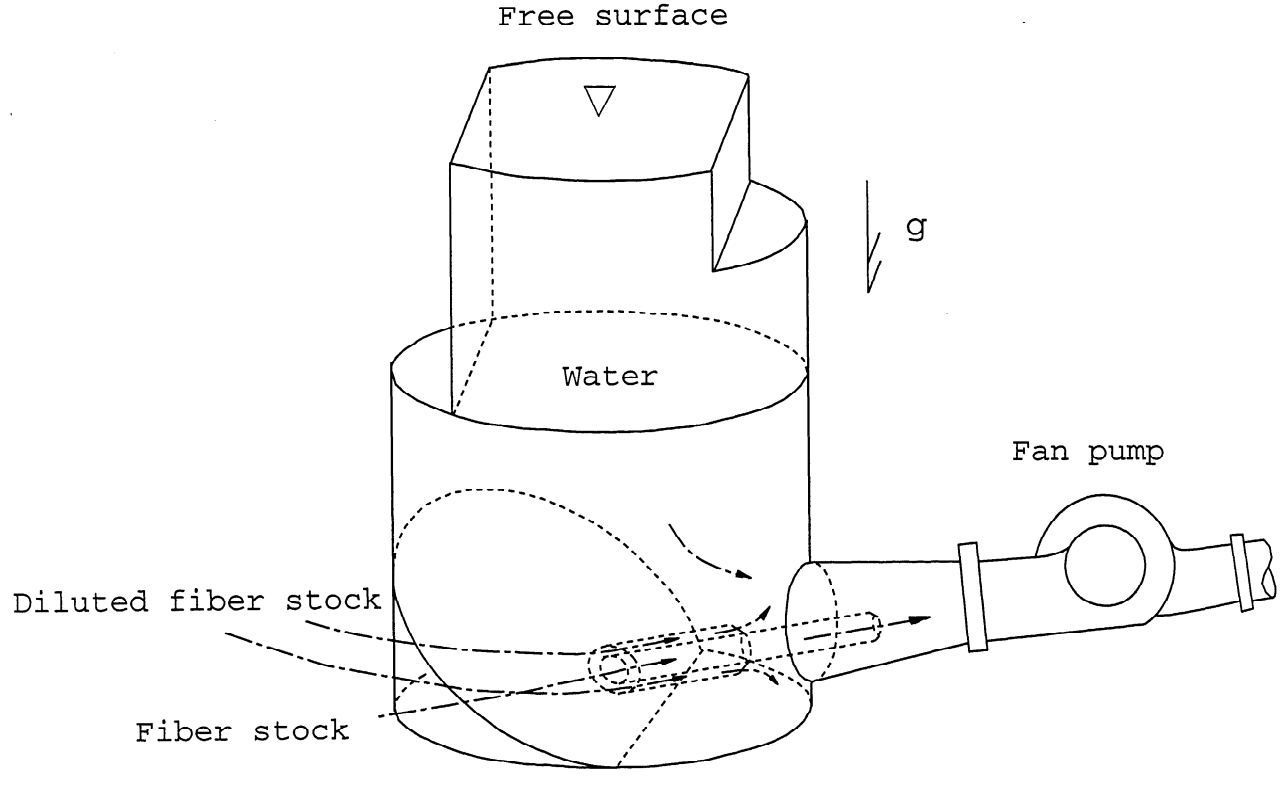

Figure 1: Location of the mixing pipe in the silo unit.

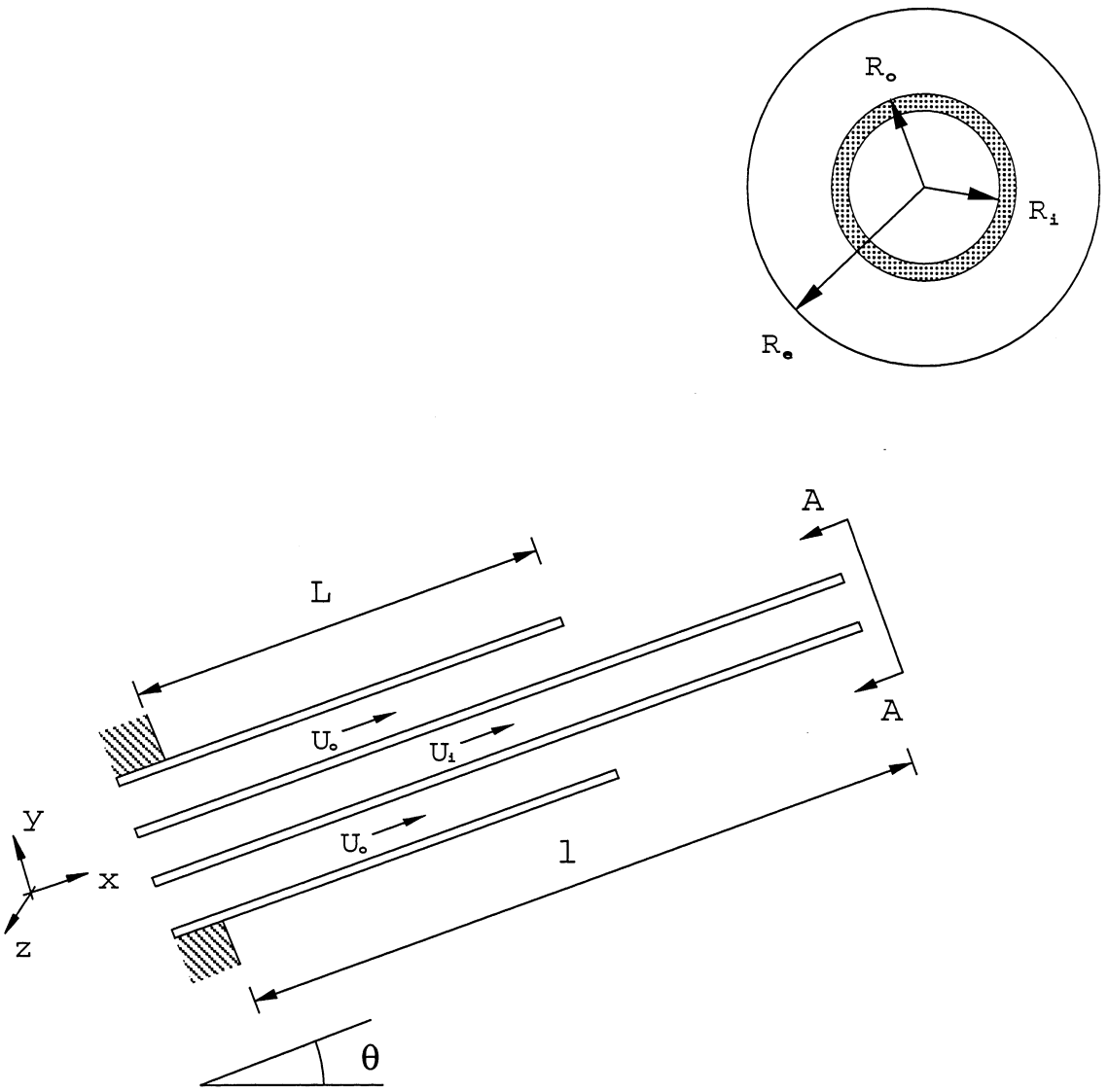

Figure 2: The concentric piping equilibrium configuration.

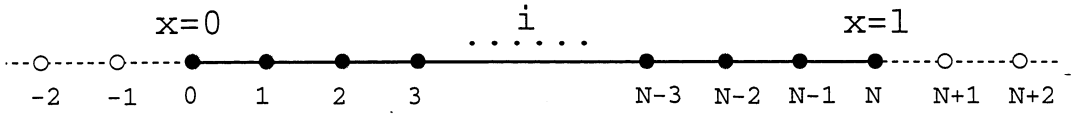

Figure 3: Finite difference stations on the tubular beam.

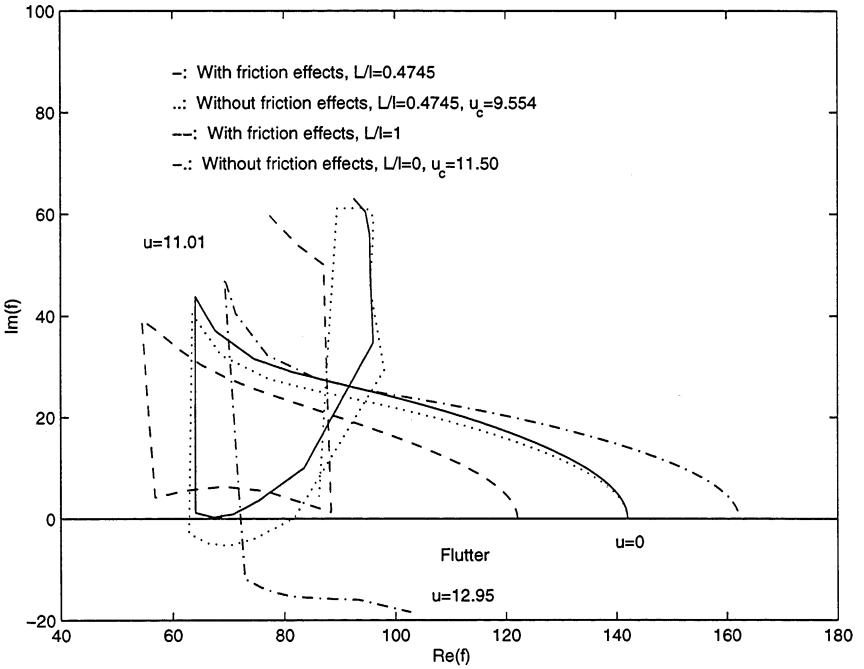

Figure 4: Flutter instability of the fourth mode with $U_i/U_e = 1.7$. (Twenty-one grid points.)

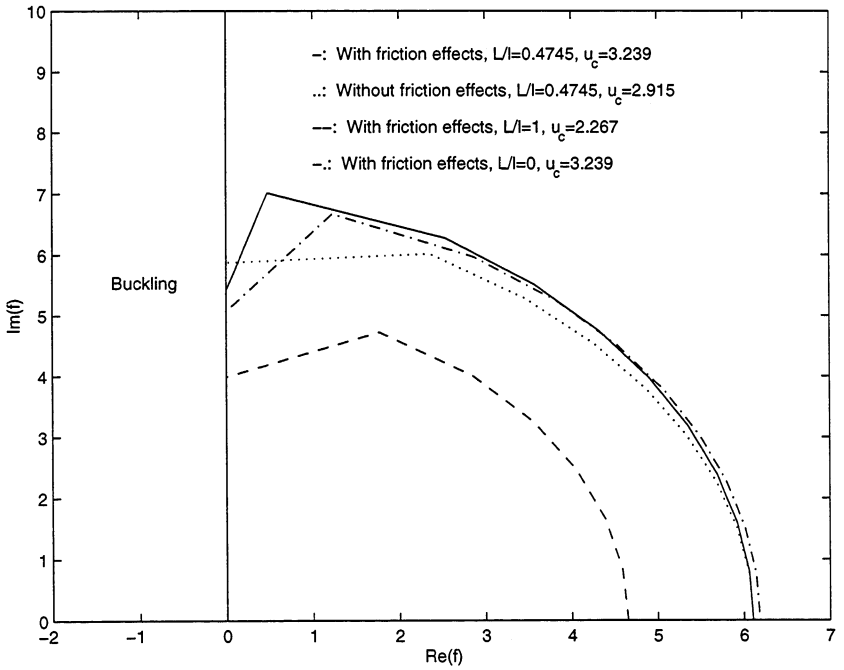

Figure 5: Buckling instability of the first mode with $U_i/U_e = 1.7$. (Twenty-one grid points.)

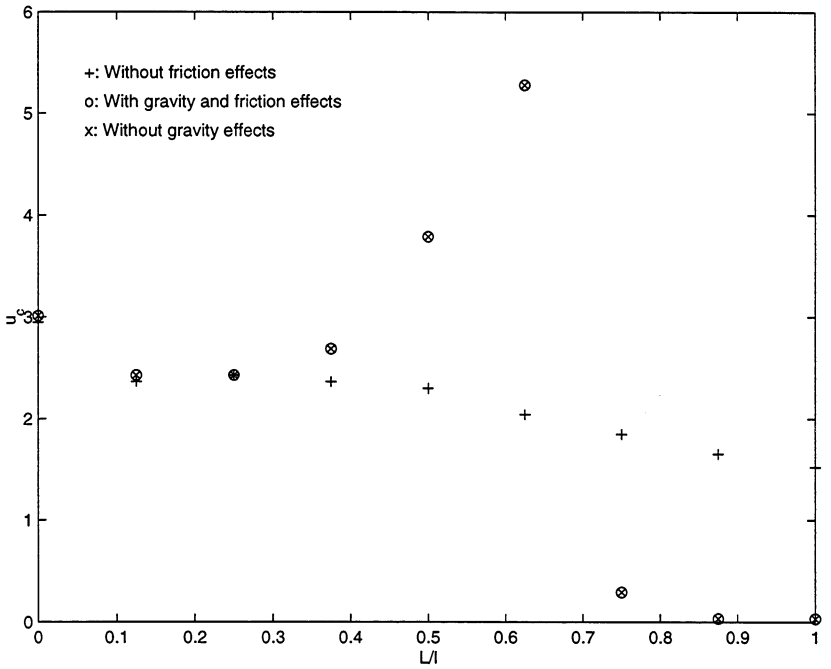

Figure 6: Critical buckling velocity *vs.* the outer pipe length with $U_i/U_e = 1.7$. (Twenty-one grid points.)

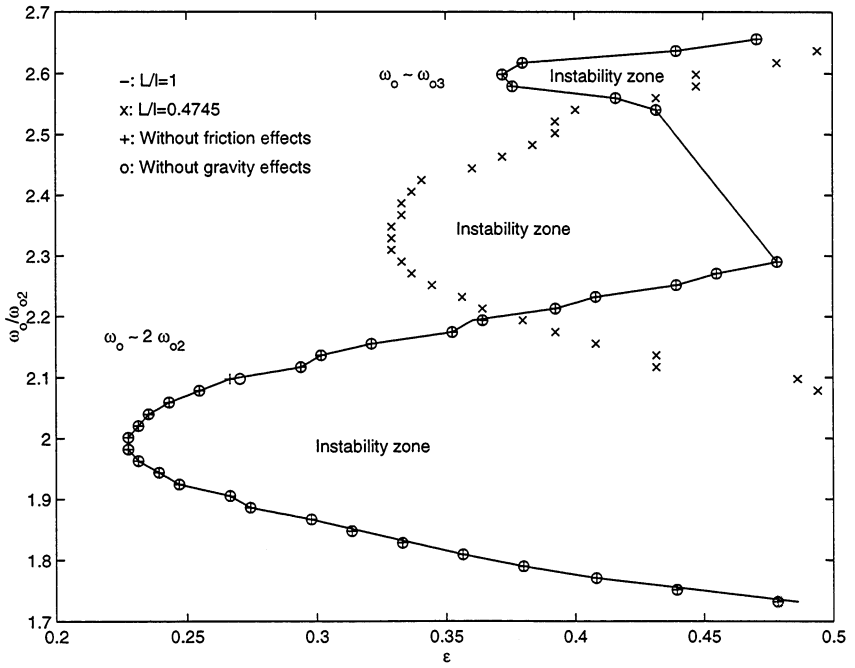

Figure 7: Dynamic instability regions. ($\omega_{o1} = 26.13$ rad/s and $\omega_{o2} = 117.3$ rad/s with five grid points.)

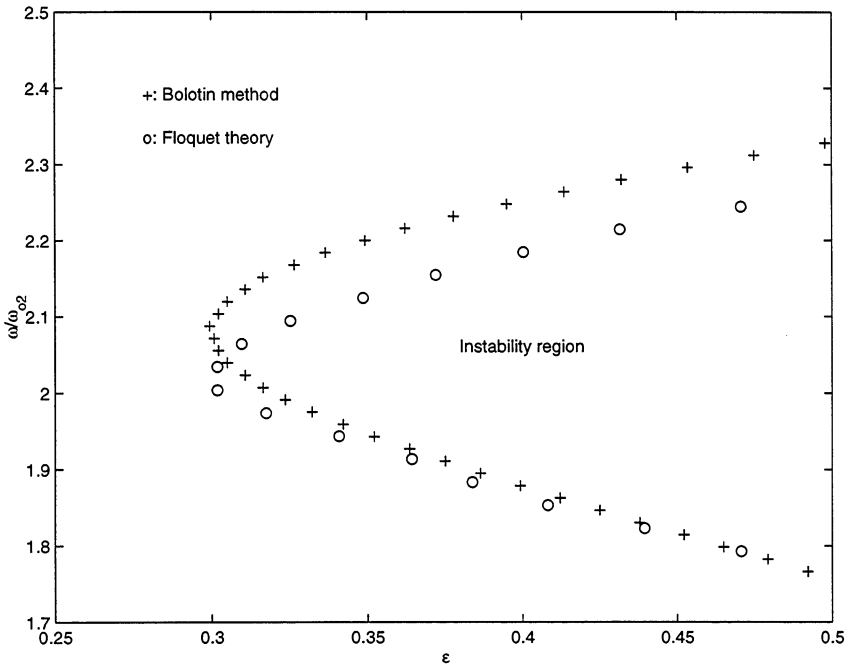

Figure 8: Results derived from the Floquet theory and the Bolotin method. (Eleven grid points for spatial discretization.)

References

[1] S.T. Ariaratnam and N.S. Namachchivaya. Dynamic stability of pipes conveying pulsating fluid. *Journal of Sound and Vibration*, 107(2):215–230, 1986.

[2] H. Ashley and G. Haviland. Bending vibrations of a pipe line containing flowing fluid. *Journal of Applied Mechanics*, 17:229–232, 1950.

[3] K.J. Bathe. *Finite Element Procedures.* Prentice Hall, Englewood Cliffs, N.J., 1996.

[4] T.B. Benjamin. Dynamics of a system of articulated pipes conveying fluid. I. Theory. *Proceedings of the Royal Society, Series A*, 261:457–486, 1961.

[5] T.B. Benjamin. Dynamics of a system of articulated pipes conveying fluid. II. Experiments. *Proceedings of the Royal Society, Series A*, 261:487–499, 1961.

[6] R.D. Blevins. *Formulas for Natural Frequency and Mode Shape.* Van Nostrand Reinhold Company, 1979.

[7] V.V. Bolotin. *The Dynamic Stability of Elastic Systems.* Holden-Day, 1964.

[8] S.S. Chen. Dynamic stability of tube conveying fluid. *Journal of the Engineering Mechanics Division ASCE*, 97:1469–1485, 1971.

[9] J.H. Ginsberg. The dynamic stability of a pipe conveying a pulsatile flow. *International Journal of Engineering Science*, 11:1013–1024, 1973.

[10] R.W. Gregory and M.P. Paidoussis. Unstable oscillation of tubular cantilevers conveying fluid I. theory. *Proceedings of the Royal Society, Series A*, 293:512–527, 1966.

[11] M.J. Hannoyer and M.P. Paidoussis. Instabilities of tubular beams simultaneously subjected to internal and external axial flows. *ASME Journal of Mechanical Design*, 100:328–336, 1978.

[12] S.T. Noah and G.R. Hopkins. Dynamic stability of elastically supported pipes conveying pulsating fluid. *Journal of Sound and Vibration*, 71(1):103–116, 1980.

[13] M.P. Paidoussis. Dynamics of flexible slender cylinders in axial flow. Part 1. Theory. *Journal of Fluid Mechanics*, 26:717–736, 1966.

[14] M.P. Paidoussis. Dynamics of cylindrical structures subjected to axial flow. *Journal of Sound and Vibration*, 29(3):365–385, 1973.

[15] M.P. Paidoussis and N.T. Issid. Dynamic stability of pipes conveying fluid. *Journal of Sound and Vibration*, 33(3):267–294, 1974.

[16] M.P. Paidoussis and G.X. Li. Pipes conveying fluid: A model dynamical problem. *Journal of Fluids and Structures*, 7:137–204, 1993.

[17] M.P. Paidoussis and M.J. Pettigrew. Dynamics of flexible cylinders in axisymetrically confined axial flow. *Journal of Applied Mechanics*, 46:37–44, 1979.

[18] M.P. Paidoussis and C. Sundararajan. Parametric and combination resonances of a pipe conveying pulsating fluid. *Journal of Applied Mechanics*, pages 780–783, December 1975.

[19] H. Schlichting. *Boundary-Layer Theory.* McGraw-Hill, seventh edition, 1987.

[20] G. Taylor. Analysis of the swimming of long and narrow animals. *Proceedings of the Royal Society, Series A*, 214:158–183, 1952.

[21] X. Wang and F. Bloom. Dynamics of a submerged and inclined concentric pipe system with internal and external flows. *Journal of Fluids and Structures*, 1998. In press.

[22] X. Wang, Z. Feng, and L.J. Forney. Computational simulation of turbulent mixing with mass transfer. *Computers & Structures*, 70(4):447–465, 1998.

[23] X. Wang and J.K. Hale. On monodromy matrix computation. *Center for Dynamical Systems & Nonlinear Studies*, Report CDSNS98-30, 1998. Georgia Institute of Technology.

[24] O.C. Zienkiewicz. *The Finite Element Method.* McGraw-Hill Publishing Company, third edition, 1977.